Modeling of Multiscale Solar Dynamics for Understanding Drivers of Space Weather

Irina N. Kitiashvili[1], Alan A. Wray[1], Viacheslav M. Sadykov[2], Alexander G. Kosovichev[1,3]

[1]NASA Ames Research Center, [2]Georgia State University, [3]New Jersey Institute of Technology

Understanding the solar dynamics is critical for improving our capabilities to forecast the evolution of space weather conditions. We take advantage of currently available computational capabilities to model solar dynamics from the deep interior to the corona and investigate mechanisms that may drive space weather conditions. The simulations are performed using the 3D radiative MHD code StellarBox. Comparison of synthetic spectroscopic observables obtained from numerical simulations and actual observations allows us to uncover physical processes associated with observed phenomena. To facilitate a transition from modeling short-term physical phenomena to developing a reliable forecast-oriented model, we suggest using the data assimilation approach. It allows us to cross-analyze dynamo model solutions and observations and to consider possible uncertainties and errors. In this presentation, we briefly summarize current multi-scale modeling capabilities and results and discuss ongoing developments to build a reliable physics-based forecast-oriented model of solar activity.

Modeling of self-organization processes in the solar corona

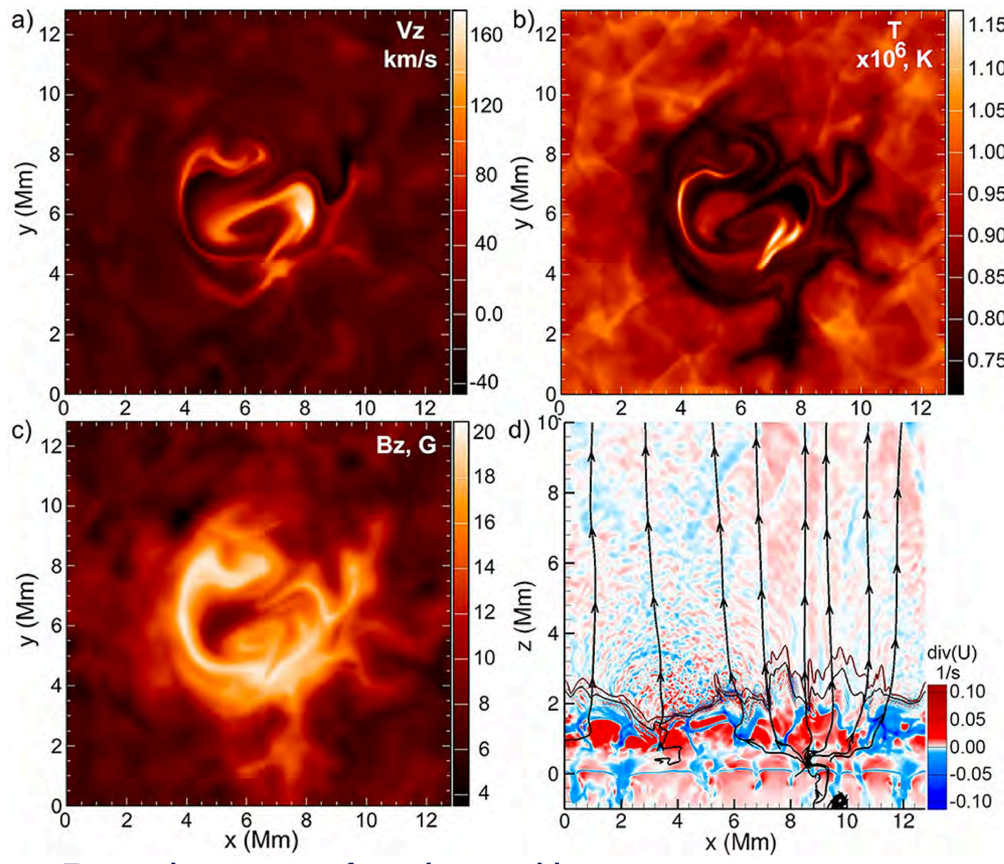

Distributions of a) vertical velocity, b) temperature, and c) magnetic field in a quiet Sun region at height 10 Mm above the photosphere. The vertical slice in panel d) shows propagation of high-frequency perturbations of velocity divergence from the transition zone to the upper layers of the corona. Color curves in panel d) correspond to temperatures of the transition region of 0.1MK and 0.5MK. Black streamlines with arrows indicate magnetic field lines. Kitiashvili et al., 2020.

Entrophy transport from the transition zone to the corona

# Eruption	Entrophy transport speed, km/s
1	16	110
2	16	76
3	30	79
4	35	115

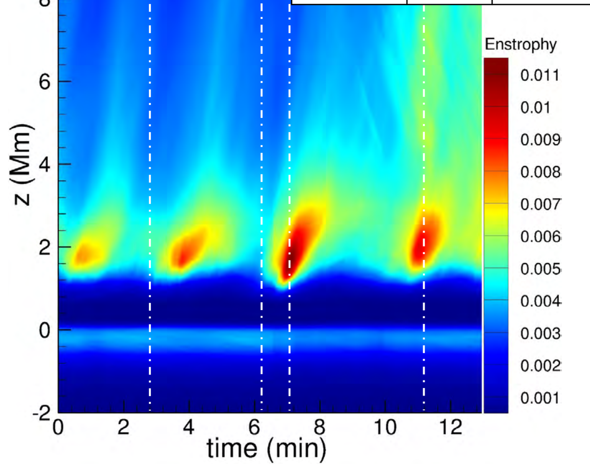

Top view of magnetic structure in solar corona

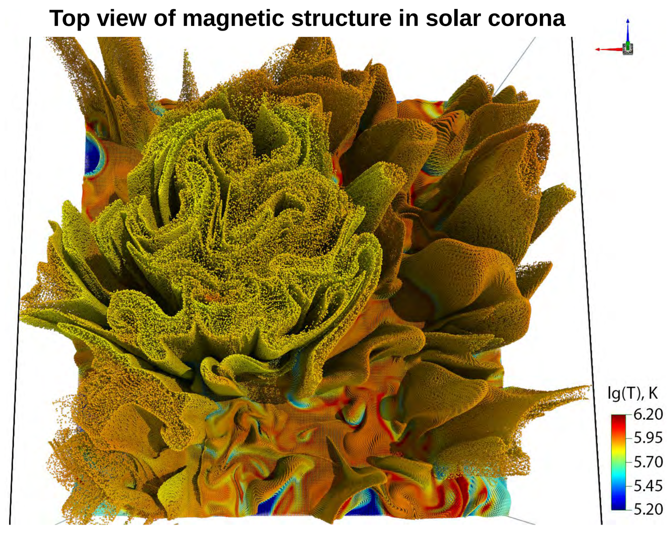

View through the solar atmosphere from the corona towards the transition zone and corona. The simulation results show a self-formed magnetic structure in the corona that is connected with kilogauss magnetic field in the photosphere through the chromosphere and transition zone. Visualization is performed by advecting particles seeded at height 2.4Mm above the solar surface.

Synthetic AIA emission in four channels calculated with the numerical (N) and instrumental (I) resolutions, and for two views at the disc center and the limb

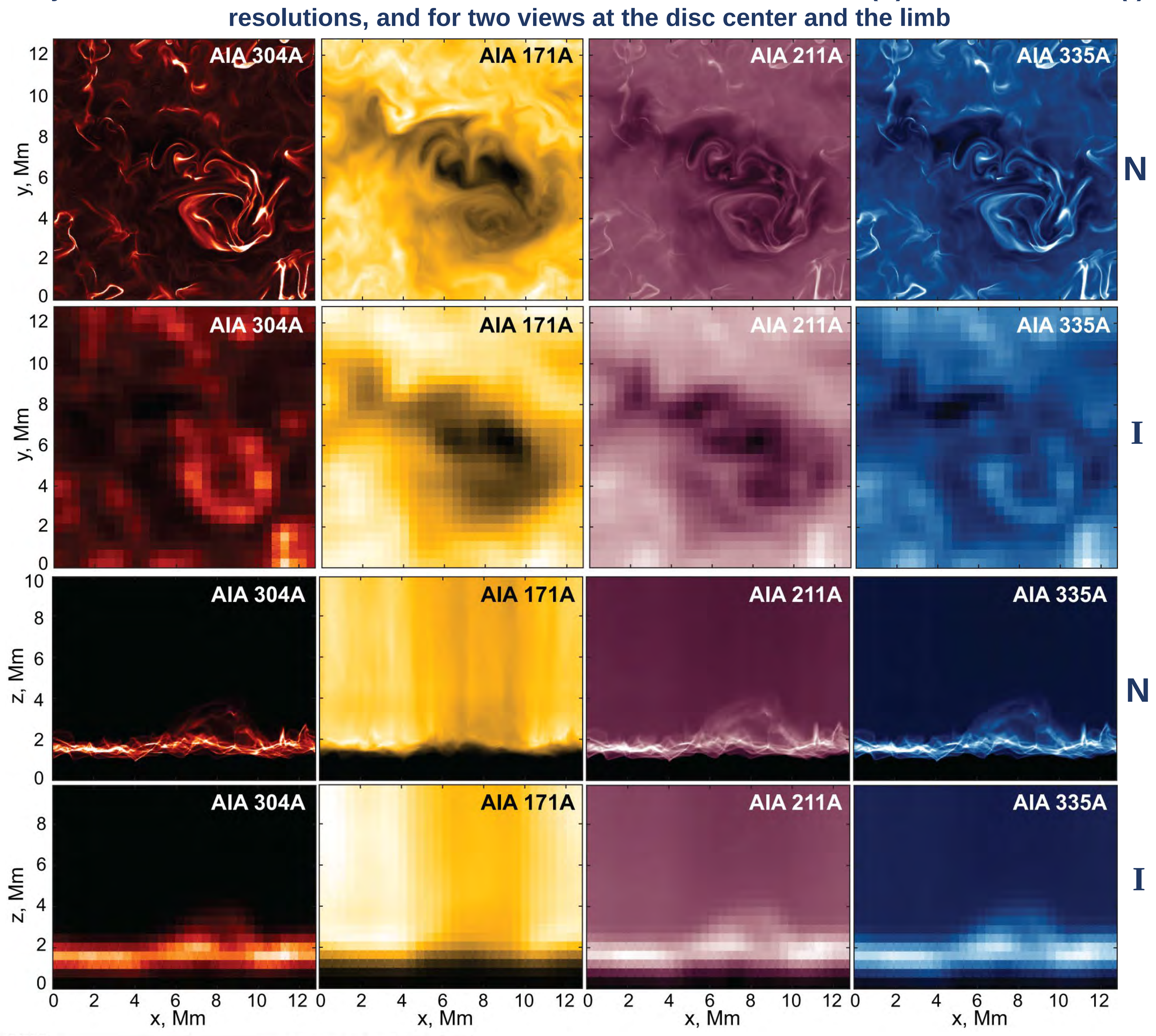

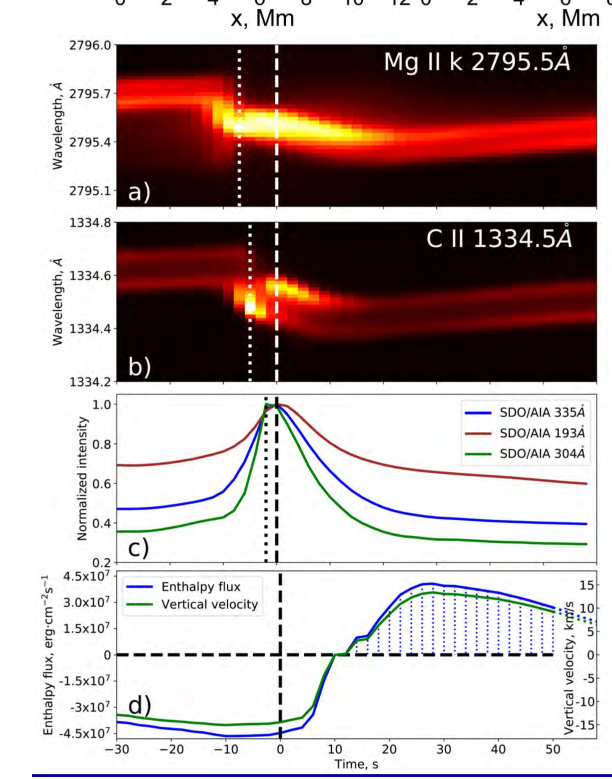

Evolution of a) the Mg II k line spectra, b) CII 1334.5A line spectra, c) normalized SDO/AIA emission, and d) physical parameters in the transition region (at the height corresponding to 5x10⁵K). The vertical dashed lines mark the time moment corresponding to the strongest SDO/AIA 335A emission during the shock. The vertical dotted lines mark the time moments of the Mg II k intensity peak (panel a), CII 1334.5A intensity peak (panel b), and SDO/AIA 304A peak (panel c). The dotted area in panel (d) indicates the positive enthalpy flux. Sadykov et al., 2021.

To investigate the underlying physical processes, we performed 3D radiative MHD simulations taking into account all essential physics and employing sub-grid scale turbulence models and reproduce the local dynamo process, spontaneous flow eruptions, coronal structure and dynamics in the quiet-Sun. Using advanced 3D radiative MHD code "StellarBox" has performed high-resolution simulations of the Sun from the convection zone to the corona. It is found that the transition zone between the low temperature (10^4 K) chromosphere and hot (10^6 K) corona is substantially more turbulent and dynamic than previously assumed. The simulations revealed new processes of generation shocks and plasma eruptions, and showed that the transition region dynamics is a source of the corona expansion and formation of the solar wind.

Modeling of Leptocline as a Shallow Substructure of Near-Surface Shear Layer (NSSL)

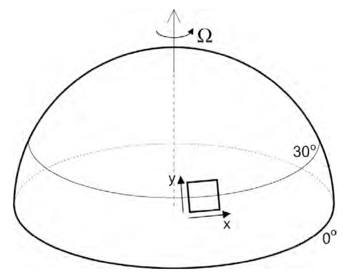

Scheme of the computation box location relative to the Sun's equator and rotation axis.

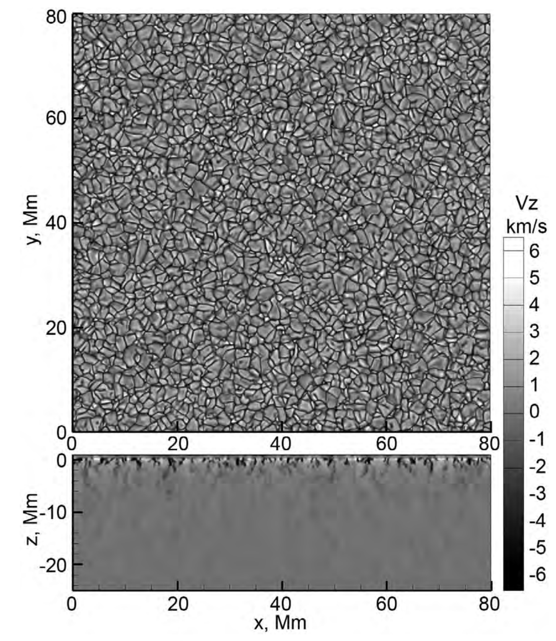

Snapshot of the vertical velocity at the solar photosphere (top panel) and a vertical slice through the computational domain (bottom).

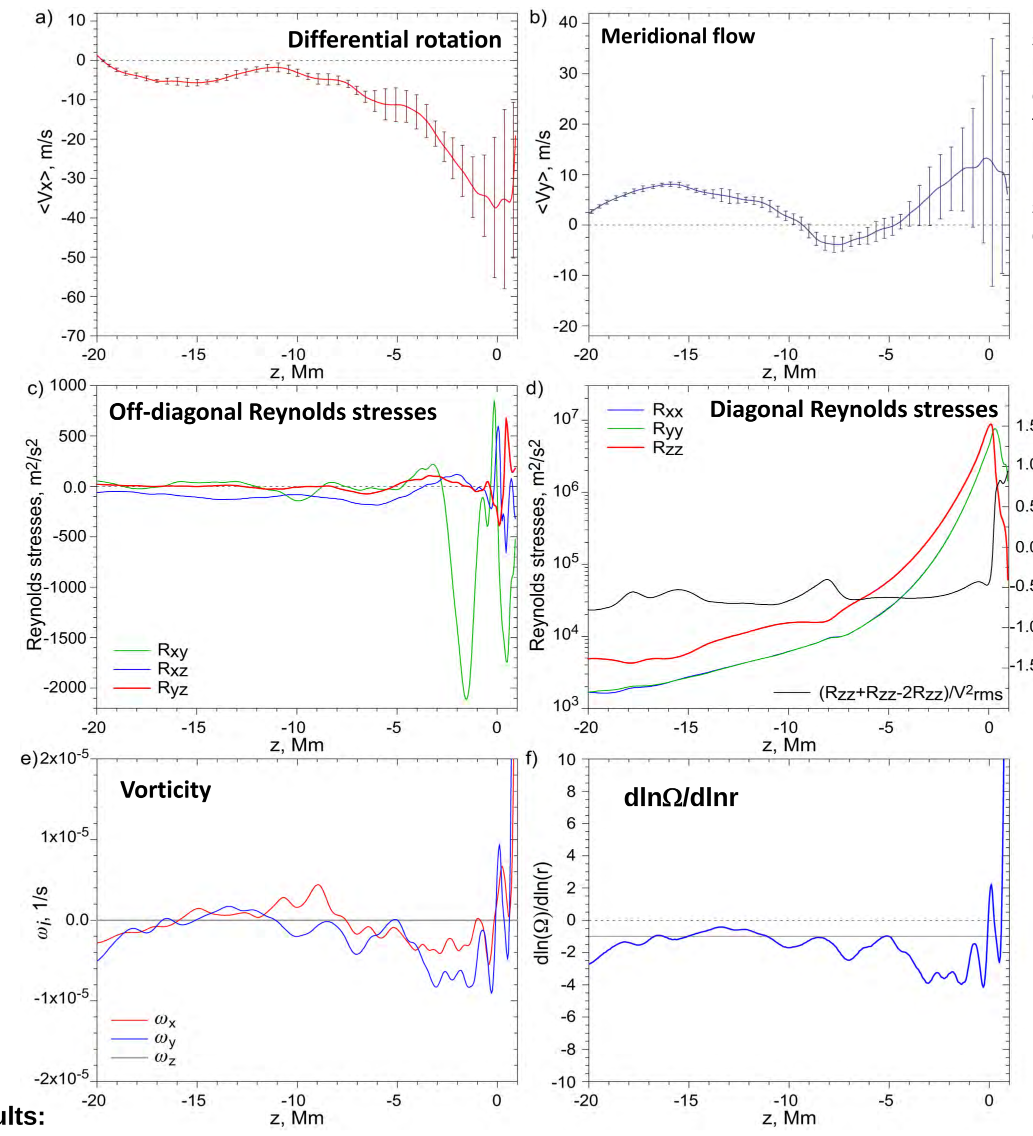

Mean radial profiles of a) deviations of the azimuthal flow speed from the imposed rotation rate at 30 degrees latitude, b) the meridional component of the flow velocity, c-d) radial profiles of the Reynolds stress components, e) the vorticity components, and f) the radial gradient of the local solar rotation rate, defined as dlnΩ/dlnr. Radial profiles are obtained by averaging a 24-hour series of simulation data. Panels a) and b) show 1σ flow velocity deviations from the mean values. Kitiashvili et al., 2022

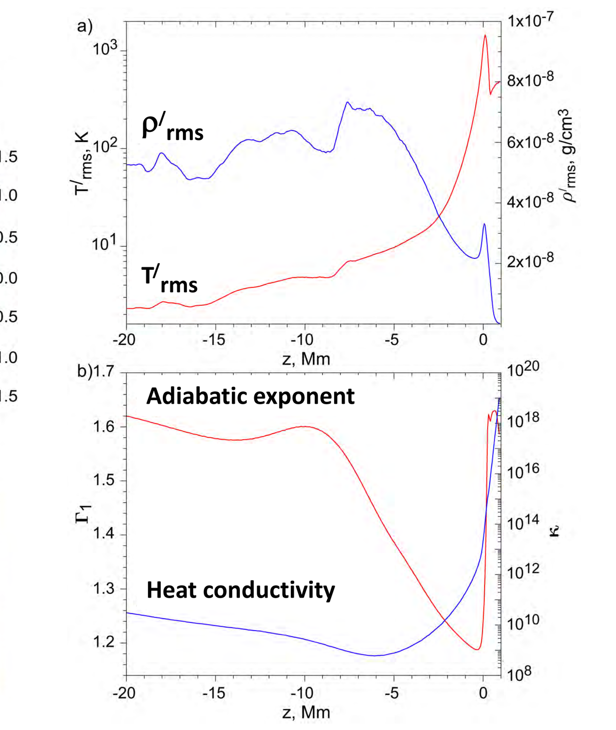

Panel a: Radial profiles of the temperature perturbations, T'_{rms} (red curve), and density perturbations, ρ'_{rms} (blue curve). Panel b: Radial profiles of the adiabatic index, Γ_1 (red curve) and the heat conductivity (blue curve).

To summarize the presented analysis of the 3D radiative hydrodynamics simulations with imposed rotation corresponding to 30 degrees latitude, we can identify the following main results:

1. The simulations reveal the development of radial differential rotation and formation of a ~10Mm-thick substructure of the Near-Surface Shear Layer (NSSL) - the leptocline - associated with a steep radial gradient of the angular velocity, changes in the thermodynamic and structural properties of the convection, and the bottom of the hydrogen ionization zone.

2. The leptocline constitutes the upper part of NSSL. The interface between the leptocline and deeper layers is characterized by overshooting downdrafts, which may intensify the turbulent mixing below the leptocline layer.

3. The self-formed meridional flows are characterized by poleward mean motions near the photosphere and weak reverse flows at depths of 5 – 10 Mm. The bottom of the reverse flows corresponds to the bottom of the leptocline layer and the hydrogen ionization zone. This structure resembles a double-cell meridional circulation previously found on the whole-convection-zone scale.

'StellarBox' code (Wray et al., 2015;2018)

- ✓ 3D rectangular geometry
- ✓ Fully conservative, Fully compressible
- ✓ Fully coupled radiation solver:
  - LTE using 4 opacity-distribution-function bins
  - Ray-tracing transport by Feautrier method
  - 18 ray angular quadrature
- ✓ Non-ideal (tabular) EOS
- ✓ 4th order Padé spatial discretization
- ✓ 4th order Runge-Kutta time integration
- ✓ Turbulence models: compressible Smagorinsky model, compressible Dynamics Smagorinsky model (Germano et al., 1991; Moin et al., 1991), MHD subgrid models (Balarac et al., 2010), DNS+Hyperviscosity approach
- ✓ MPI parallelization (plane and pencil versions)

Comparison of meridional circulation from helioseismic inferences at 30 degrees latitude (panel a) and model (panel b).

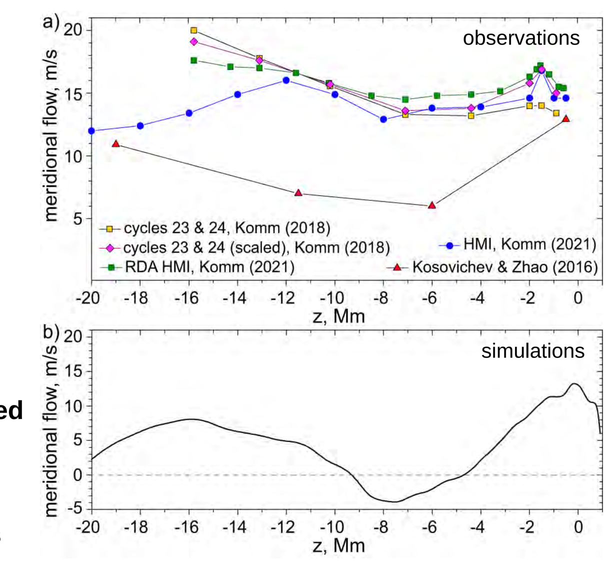

Prediction of Solar Global Activity

Dynamo model

$$\frac{\partial A}{\partial t} = \alpha B + \eta \nabla^2 A \qquad \alpha_k = -(\tau/3)\langle \mathbf{u}(\nabla\times\mathbf{u})\rangle$$

$$\frac{\partial B}{\partial t} = G\frac{\partial A}{\partial z} + \eta\nabla^2 B \qquad \alpha_m = (\tau/12\pi\rho)\langle \mathrm{h}(\nabla\times\mathrm{h})\rangle$$

$$\alpha = \alpha_k + \alpha_m$$

$$\frac{\partial \alpha_m}{\partial t} = \frac{\mu}{4\pi\rho}\left(\mathbf{B}\cdot(\nabla\times\mathbf{B}) - \frac{\alpha B^2}{\eta}\right) - \frac{\alpha_m}{T_\alpha}$$

Data Assimilation Methodology

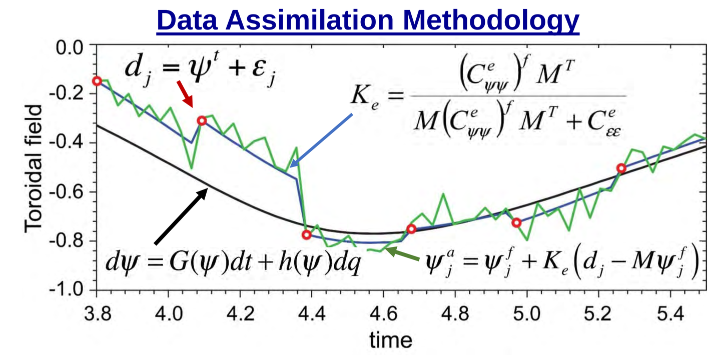

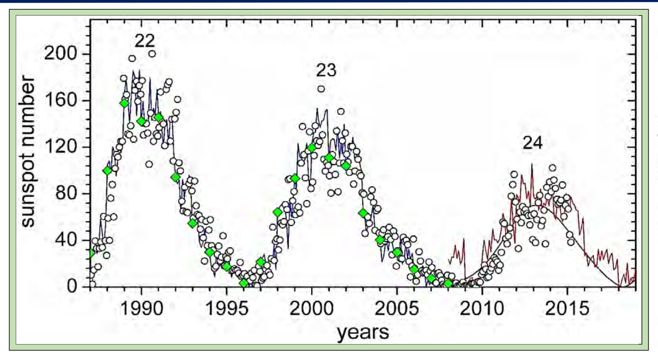

Comparison of the sunspot number prediction for SC24 (red curve, Kitiashvili & Kosovichev, 2008) and actual observations of monthly sunspot number. The blue curve shows the corrected dynamo solution according to annual sunspot number (green diamonds).

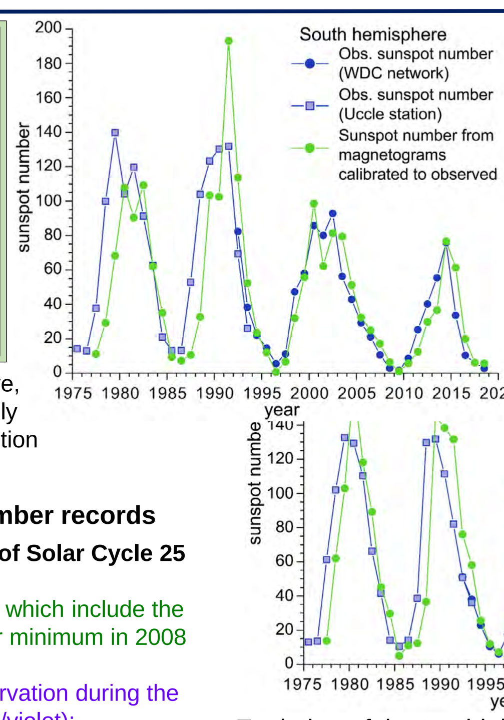

Comparison of hemispheric sunspot numbers, observed and inferred from magnetograms

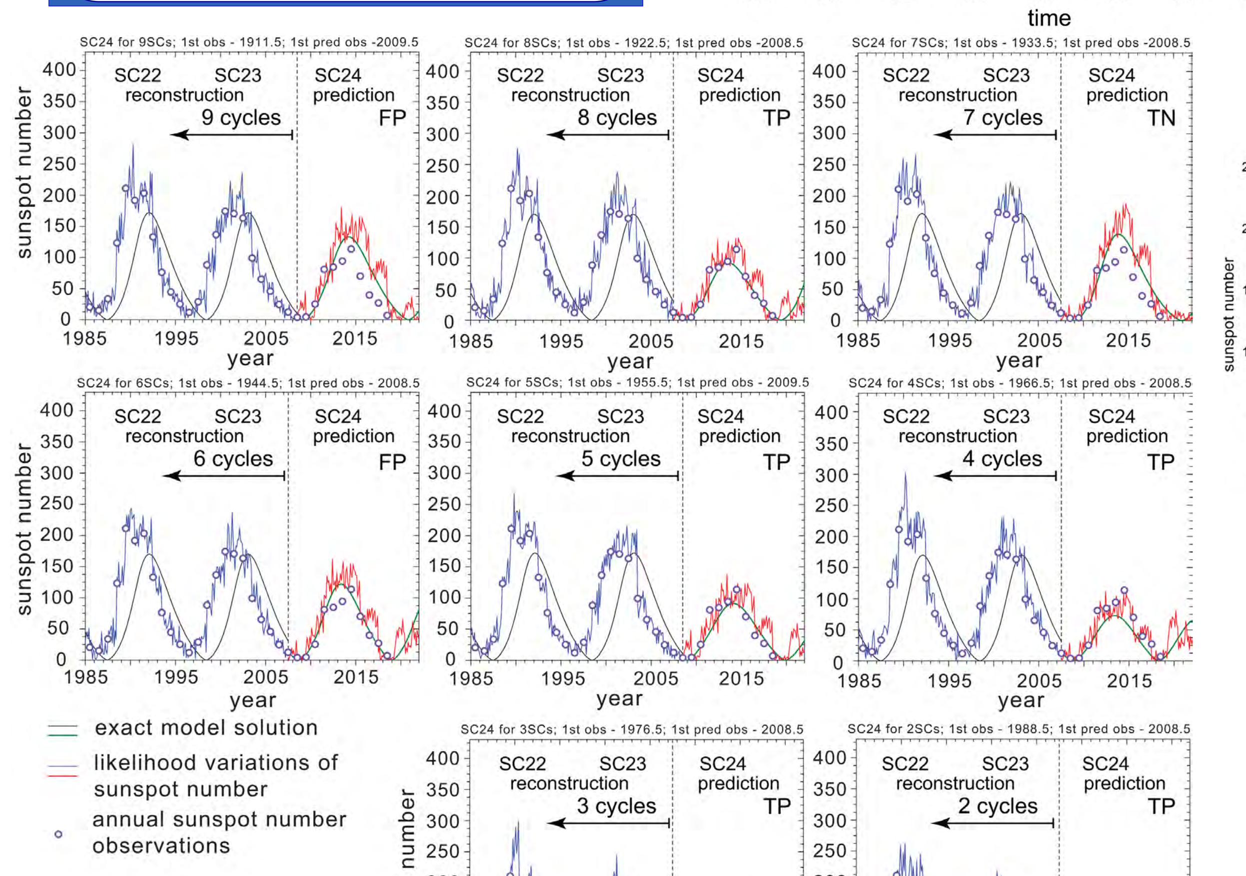

Black and green curves show the exact model solutions for the reconstruction and prediction phases. Blue and red curves correspond to the likelihood variations of the sunspot number. The actual annual sunspot number indicated by circles. The panels are marked according to the test case performance (e.g., true-positive, or TP, for SC19 prediction using the nine-cycles-long observational data at the upper left panel).

Uncertainties in Prediction of Solar Cycle 25 using sunspot number records

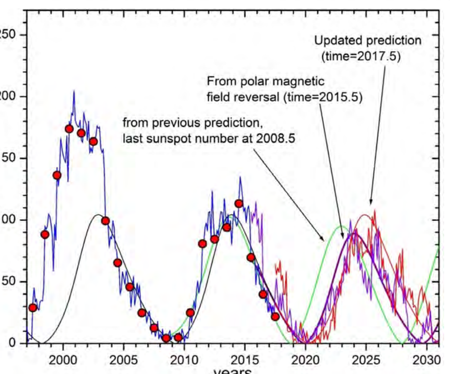

Early estimates of the properties of Solar Cycle 25 (for sunspot number version 2.0)

prediction obtained for observations which include the sunspot number data up to the solar minimum in 2008 (green curve);

prediction obtained for the last observation during the polar magnetic field reversal (purple/violet);

prediction obtained using all currently available observations up to 2017 (red curve).

Blue curve shows the best EnKF estimates of the previous cycles based on the dynamo model and all available sunspot observations (red circles).

Evolution of the mean toroidal (panel a) and poloidal (b) fields in the Northern and Southern hemispheres based on the field observations for three solar cycles, and prediction of the mean toroidal and poloidal field components variation during SC24.

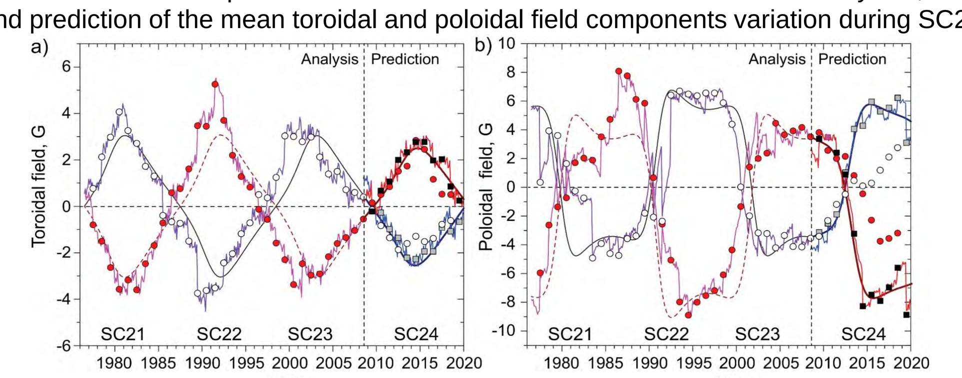

Evolution of the toroidal and poloidal magnetic fields obtained from the synoptic magnetograms

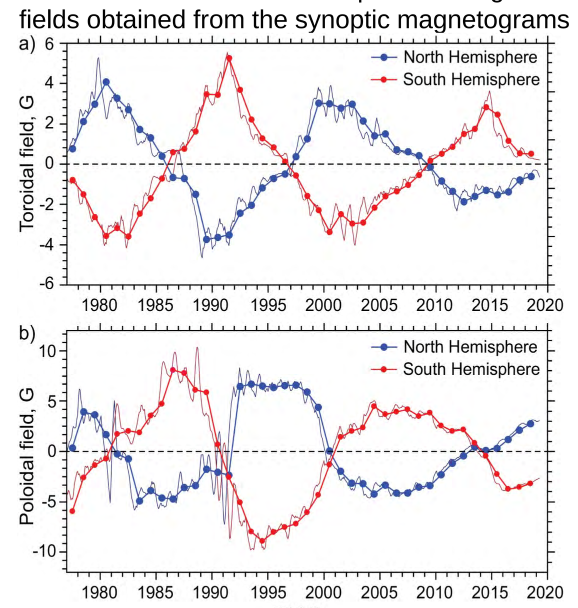

Solar Cycle 25 prediction

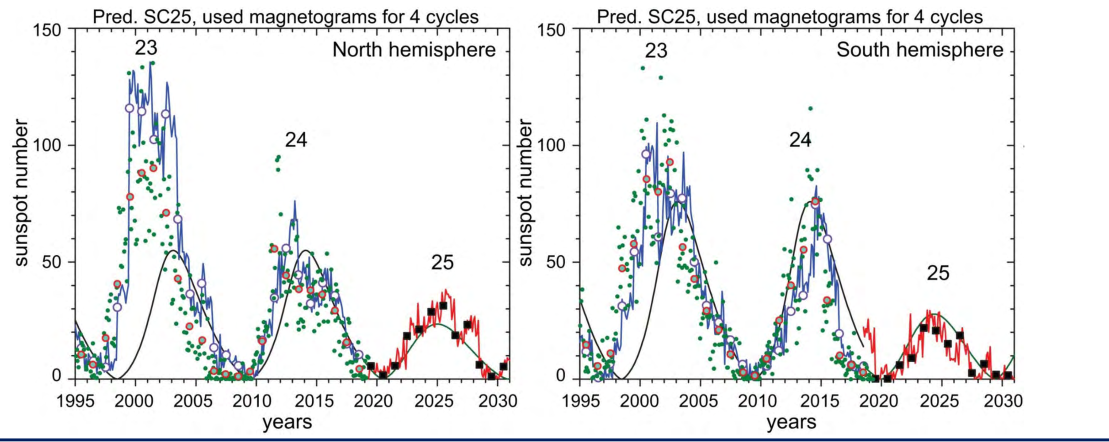

In this work we takes advantage of synoptic observations of magnetic field emerging on the surface of the Sun to develop a more advanced and reliable forecasting method. The observational data are assimilated into a non-linear dynamo model which provides a theoretical description of the generation and evolution of the global magnetic field of the Sun. Using the currently available observational data, predictions and prediction uncertainties have been calculated for Solar Cycle 25. The results based on both the sunspot number series and observed magnetic fields indicate that the upcoming Solar Maximum (Solar Cycle 25) is expected to be weaker than that of the current cycle (which near its end). The model results show that a deep extended solar activity minimum is expected in about 2019-2021, the maximum will occur in 2024 - 2025, and the mean sunspot number at the maximum will be about 50 (for the v2.0 sunspot number series) with an error estimate of ~15%. The maximum will likely have a double peak or show extended high activity over 2 – 2.5-years.

Test 'Prediction' of Solar Cycles 23 and 24 for the North and South hemispheres using the reconstructed toroidal and poloidal magnetic field components

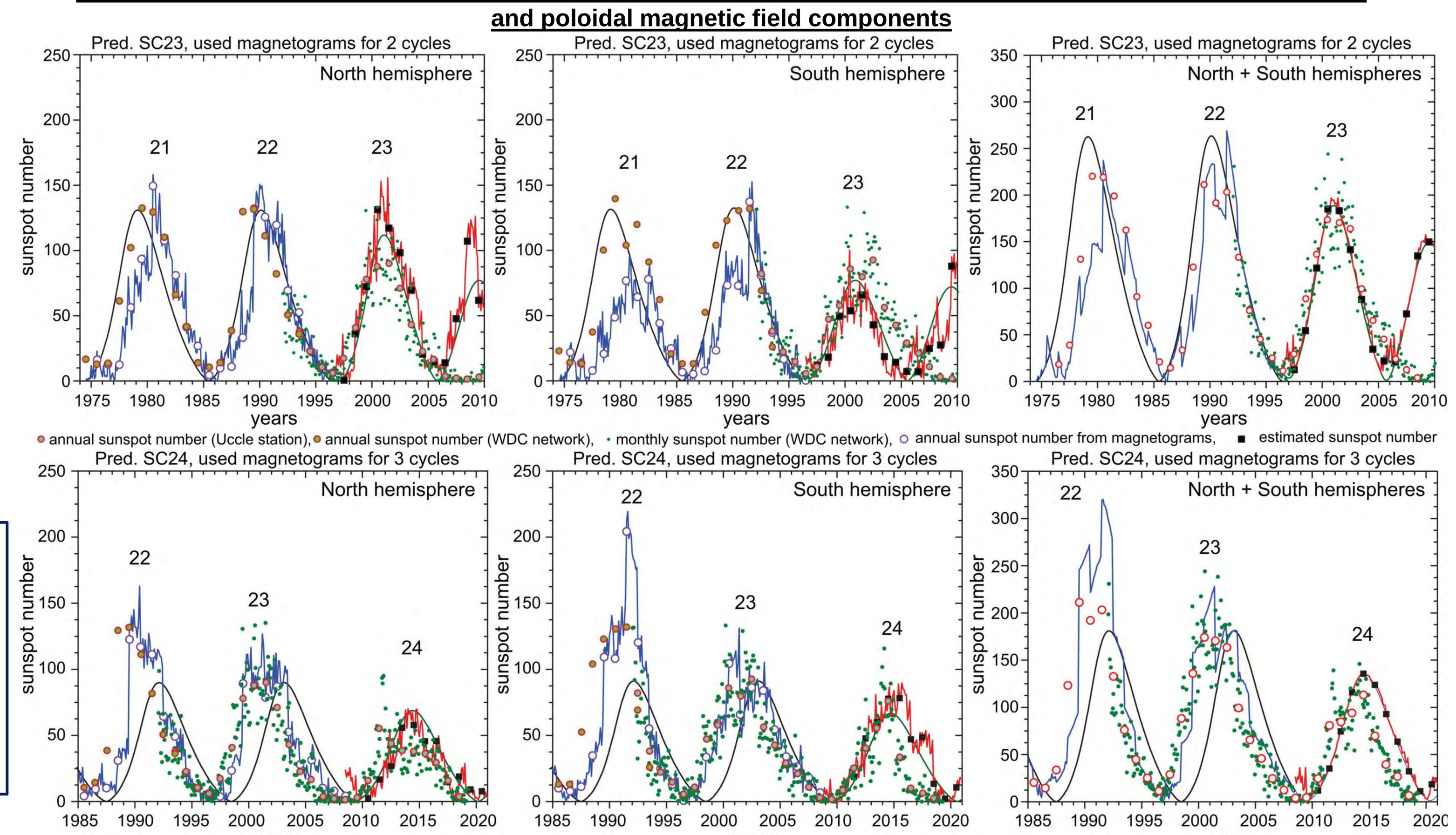

Balarac G., Kosovichev A.G., Brugière O., Wray A.A., Mansour N.N., 2010. ArXiv: 1010.5759.
Evensen G. Data Assimilation. Springer. 2007.
Germano M., Piomelli U., Moin P., et al. 1991. Physics of Fluids **3**, p.1760.
Kitiashvili I.N. 2016. ApJ 831, article id. 15.
Kitiashvili I. N. & Kosovichev A. G. 2008. ApJ 688, L49-L52.
Kitiashvili I.N. & Kosovichev A.G. 2009. GAFD 103, 53-68.

Kitiashvili, I.N. & Kosovichev, A.G. 2011. Lecture Notes in Physics 832, p121.
Kitiashvili I.N. 2016. ApJ 831, article id. 15, 8 pp.
Kitiashvili I.N., 2020. ApJ 890, id.36, 15 pp.
Sadykov V.M. ApJ 909, id.35, 14 pp.

Kitiashvili I.N., Wray A.A., Sadykov V.M., Kosovichev A.G., Mansour N.N. 2020. IAUS Proc 354, pp. 346-350.
Kitiashvili I.N., Kosovichev A.G., Wray A.A., Sadykov V.M., Guerrero G. 2022. arXiv:2203.01484
Kleeorin N.I., Ruzmaikin A.A. 1982. Magnetohydrodynamics, 18, 116.
Kleeorin N., Rogachevskii I., Ruzmaikin A. 1995. A&A 297, 159-167.

Moin P., Squires K., Cabot W., Lee, S., 1991. Physics of Fluids **3**, p.2746.
Smagorinsky, J., 1963. Monthly Weather Review 91, 99.
Wray A.A., Bensassi K., Kitiashvili I. N., Mansour N. N., Kosovichev A. G. 2015. ArXiv: 1507.07999.

Wray A.A., Bensassi K., Kitiashvili I.N., Mansour N.N, Kosovichev A.G. 2018. In Book: "Variability of the Sun and Sun-like Stars: from Asteroseismology to Space Weather". Eds: J.-P. Rozelot, E.S. Babaev, EDP Sciences, 2018. p.39-62.

The research is funded by the NASA Heliophysics Support & NASA DRIVE Centers Program